ACS OMEGA

Open Access

http://pubs.acs.org/journal/acsodf

Article

Analysis of Pollution Characteristics and Contributions of Firework Burnings in Nanchang during the Spring Festival

Changan Kang, Ruihe Lyu,* Mingbiao Luo,* Juanjuan Jia, Min Liu, Chenghua Qin, Yanzhi Peng, Bingwei Cao, Caiyu Zou, and Yao Ma

Cite This: *ACS Omega* 2024, 9, 37754−37762

Read Online

ACCESS | Metrics & More | Article Recommendations

ABSTRACT: This study investigates the impact of fireworks on air quality during the Spring Festival in Nanchang City, utilizing high-resolution monitoring data from February 7th to 15th, 2021. Significant variations in K^+ concentrations were observed, indicating severe air quality impacts. During the most intense discharge event A, K^+ concentrations were 20.7 times higher than background levels, with $PM_{2.5}$ and PM_{10} levels rising to 3.63 and 3.32 times above the background, respectively. The contribution of fireworks to $PM_{2.5}$ was determined to be 72.5 ± 25.6%. Sulfate (SO_4^{2-}) and nitrate (NO_3^-) concentrations also increased significantly, with $\Delta[SO_4^{2-}]$ and $\Delta[NO_3^-]$ accounting for 15.4 ± 18.7% and 10.9 ± 12.3% of $PM_{2.5}$, respectively. The study highlights the necessity for effective emission control strategies to mitigate the adverse effects of fireworks on urban air quality and public health. Future research should focus on the detailed chemical pathways and long-term impacts of these episodic emissions.

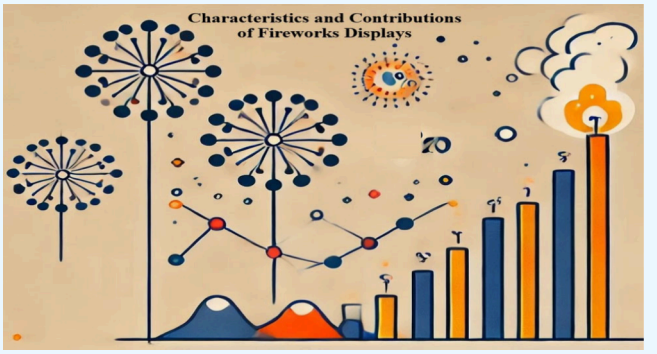

1. INTRODUCTION

$PM_{2.5}$ particles have received significant attention due to their potential impact on air quality, climate change, and human health.[1,2] In recent years, there has been a notable decrease in the occurrence of fine particulate matter pollution across the nation. The water-soluble components are abundant in $PM_{2.5}$, which includes sulfate (SO_4^{2-}) and nitrate (NO_3^-), ammonium (NH_4^+), sodium (Na^+), and chloride (Cl^-), etc., accounting for 30% to 80% of the concentration of $PM_{2.5}$.[3] In addition, the pH of $PM_{2.5}$ is influenced by the presence of specific water-soluble ions such as NH_4^+, Na^+, Cl^-, and NO_3^-. It should be noted that NH_4^+ and NaCl can increase pH levels.[4] Additionally, these ions do not directly influence $PM_{2.5}$ levels due to thermodynamic equilibrium processes involving nitrate (NO_3^-), which is a dominant $PM_{2.5}$ source[5−7] The partitioning of NH_3/NH_4^+ can also change as a function of aerosol composition and aerosol liquid water content, which can offset any decrease in aerosol pH[8,9]

The Spring Festival is one of the most important traditional festivals in China, and setting off fireworks/firecrackers has been necessary for celebrating and lasted for thousands of years. However, the air pollution conducted by fireworks has been focused in recent years at major festivals, and the concentration of particulate matter and water-soluble ions in the ambient air increases significantly during the period of fireworks/firecracker displays.[10] Ma Ying analyzed MARGA data of Guangzhou during the Spring Festival and found that the main pollutants were fine particulate matter and the concentration of K^+, Cl^-, and SO_4^{2-} sharply increases during the fireworks/firecrackers,[11] ZhaoYu conducted a study in Nanjing's banned urban areas during the Spring Festival, and the findings revealed elevated levels of Ba, K, Hg, and Pb in the air postfireworks/firecrackers.[12] It was suspected that these pollutants originated from the nearby suburbs and rural areas, and were subsequently transmitted to the urban areas.[13] There are many factors affecting air quality during the Spring Festival. In the period extending over a month before and after the Spring Festival, social and economic activities deviate from the normal pattern, accompanied by the use of fireworks and other factors. This complexity gives rise to environmental pollution during the Spring Festival. Therefore, it is crucial to investigate the characteristics and sources of air pollution during this period and establish quantifiable measures for control.

Nanchang City experiences a typical subtropical monsoon climate characterized by cold and humid winters with

Received: April 4, 2024
Revised: August 12, 2024
Accepted: August 14, 2024
Published: August 26, 2024

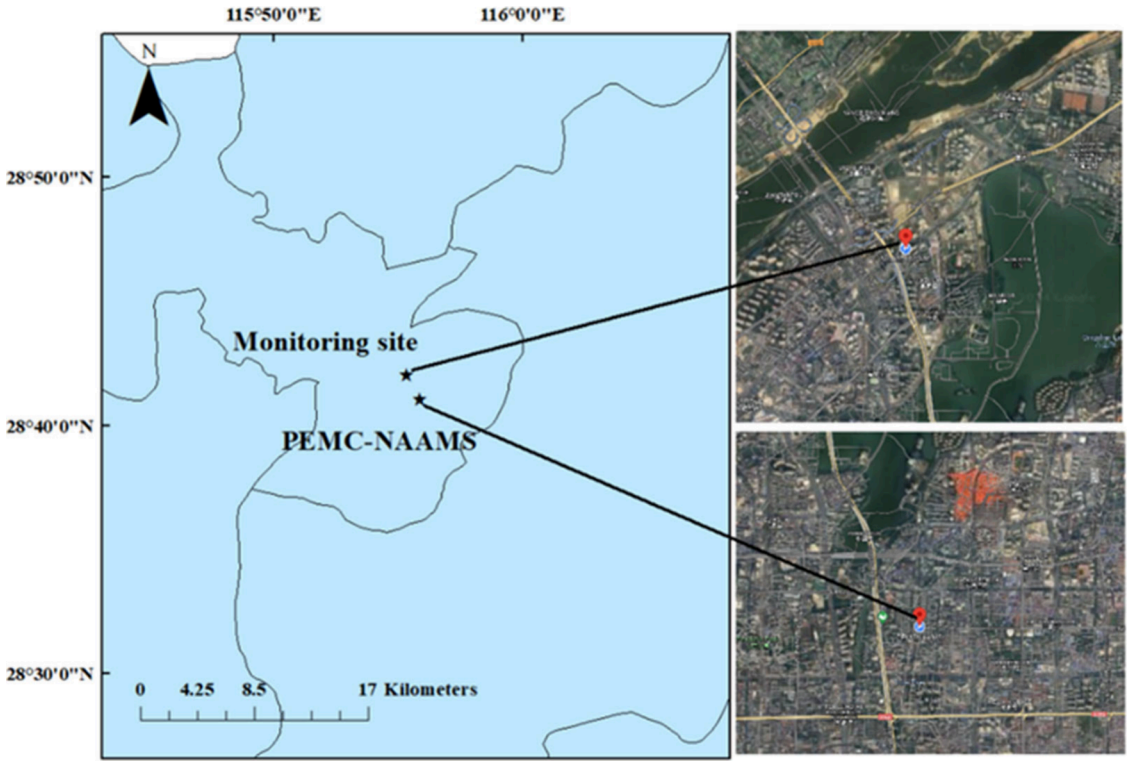

Figure 1. Location of the monitoring site and Monitoring Provincial Environmental Monitoring Center National Air Automatic Monitoring Station (PEMC-NAAMS) (map data sourced from Google Maps).

prevailing north winds. The static and stable winter weather hampers the dispersion of pollutants, leading to particulate matter pollution.[14] Lidu Town, renowned as the birthplace of fireworks/firecrackers, is situated 50 km southeast of Nanchang City's downtown area. During the Spring Festival, rural areas surrounding Nanchang City witnessed a significant rise in the popularity of fireworks/firecrackers. Due to the adverse environmental impact caused by fireworks displays, the urban area of Nanchang City, as well as neighboring counties and districts, have prohibited fireworks displays starting from January 1, 2017. This study aims to investigate the characteristics of air pollution resulting from fireworks during the Spring Festival in Nanchang City. By utilizing online high-time resolution monitoring and simulation technology in conjunction with meteorological data, the study analyzes the properties of fine particles, water-soluble ions, and secondary inorganic components during different discharge periods of air pollution.

The main contribution of fireworks is an elevated concentration of sulfate and nitrate $PM_{2.5}$, in atmospheric and the combination of high temperature and humidity during fireworks displays may facilitate the secondary formation of sulfate and nitrate.[12] This study aims to evaluate the impact of fireworks on local air quality during the Spring Festival in Nanchang City, focusing on the total contribution of fireworks to SO_4^{2-} and NO_3^-. By quantitatively examining the production of SO_4^{2-} and NO_3^- before and after fireworks discharge, this study provides a fundamental analytical framework for related research.

2. MATERIALS AND METHODS

2.1. Sampling Site. Observation point (28°42′3″ N; 115°55′20″ E) Located in the northeast of Nanchang City, it is near the Provincial Environmental Monitoring Center National Air Automatic Monitoring Station (PEMC-NAAMS)(Figure 1). The sampling port of the observation point is about 20 m high from the ground. South of the observation point is the residential area, 900 m southeast of the observation point is the lake, 1.5km north of the observation point is the Ganjiang River and agricultural land, and 80m west of the observation point is the main traffic road. The observation period of this study is from 1:00 on February 7, 2021 to 20:00 on February 15, 2021, and the atmospheric pollutants are continuously observed by online analytical instruments. It should be noted that during the observation period, fireworks are prohibited in the Nanchang urban area, and the observation point is within the urban area, which belongs to the fireworks prohibited area.

2.2. Equipment and Sources of Other Data. The concentration data of SO_2 and NO_2, $PM_{2.5}$, PM_{10} and meteorological data are obtained from the National Ambient Air Automatic Monitoring provincial station, and the pollutants concentration data are hourly concentration data.

MARGA(Monitor for Aerosols and Gases in ambient Air) aerosol and gas component online ion chromatography detection system (Valton, Switzerland) for real-time monitoring of water-soluble ion components in gases and $PM_{2.5}$. Among them, cations include Na^+, K^+, NH_4^+, Mg^{2+} and Ca^{2+}; Anions include Cl^- and SO_4^{2-} and NO_3^-. The online monitoring system completes sampling and sample determination every hour. The online monitoring system includes a $PM_{2.5}$ sampler, a gas and aerosol collection device, and an ion chromatography analysis system (ICS-1100). The samples collected online were extracted by ultrapure water, filtered by 0.45 μm microporous filter membrane, and then entered ICS-1100 ion chromatography by automatic sampling.

https://doi.org/10.1021/acsomega.4c03237
ACS Omega 2024, 9, 37754−37762

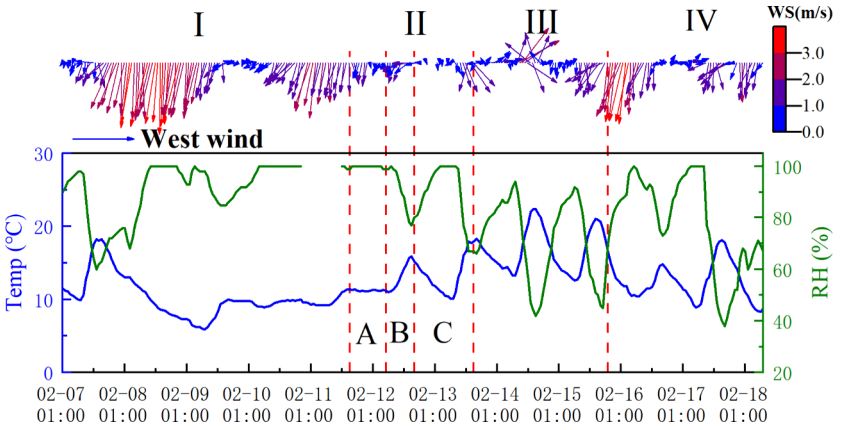

Figure 2. Hourly variations in meteorological factors (temperature, relative humidity, wind direction, and wind speed) during observation periods: A, B, and C (fireworks discharge event); I and IV (nondischarge periods); II (concentrated discharge period); and III (discharge impact period).

The analysis column model CS12A and the protection column model CG12A were used for the determination of conventional cationic components. The eluent was methylsulfonic acid (MSA) solution (15 mmol/L). The pump flow rate was 0.25 mL/min, the suppressor current value was 12 mA, and the analysis time was 26.5 min.

The analytical column model used for determining conventional anionic components is AS11-HC, the protective column model is AG11-HC, and the eluent is KOH solution (0−33 mmol/L). The eluent method is gradient elution, with a pump flow rate of 0.38 mL/min, a suppressor current value of 29 mA, and an analysis time of 26.5 min.

The column temperature of the cationic and anionic analysis column was set at 30 °C, the detection limit of the system was less than 0.1 $\mu g/m^3$, and the standard solution was prepared as needed.

3. RESULTS AND DISCUSSION

3.1. Meteorological Observation Results. Figure 2 presents the average hourly values of meteorological variables throughout the observation period. The data were discontinuous due to missing data in certain periods. The temperature and relative humidity were both high during the monitoring period, with an average temperature of 12.4 ± 3.52 °C and an average relative humidity (RH) of 87.6 ± 16.7%. From February seventh to February 12th at 16:00, there were relatively small changes in temperature and RH, with an average of 10.7 ± 2.66 °C and 92.0 ± 11.1%. In the later part of the monitoring period, there were significant fluctuations in temperature and RH, with an average of 14.2 ± 2.15 °C and 77.4 ± 8.79%. Research conducted by Cheng et al. revealed that the heterogeneous reactions are considerably inhibited when the temperature drops below 0 °C in the absence of a particle surface water film.[15] The high temperature and humidity conditions observed during the study period were conducive to the formation of secondary particulate matter through heterogeneous reactions in the atmosphere. The average wind speed during the observation period was 1.26 ± 0.89 m/s, and the frequency of calm wind was about 3%, the frequency of wind speed below 1 m/s reached 42.3%. The northerly winds were dominant direction, and the frequency of the north wind reached 71%, facilitating the observation of the transport of atmospheric particles from the northern region to the central city.

3.2. Analysis of Observations of Water-Soluble Ions and Particulate Matter. The monitoring period was divided into four distinct periods based on abrupt fluctuations observed in monitoring data, and also considering both the conventional timing of fireworks displays and the regulations prohibition these displays (Figure 3): nondischarge period I

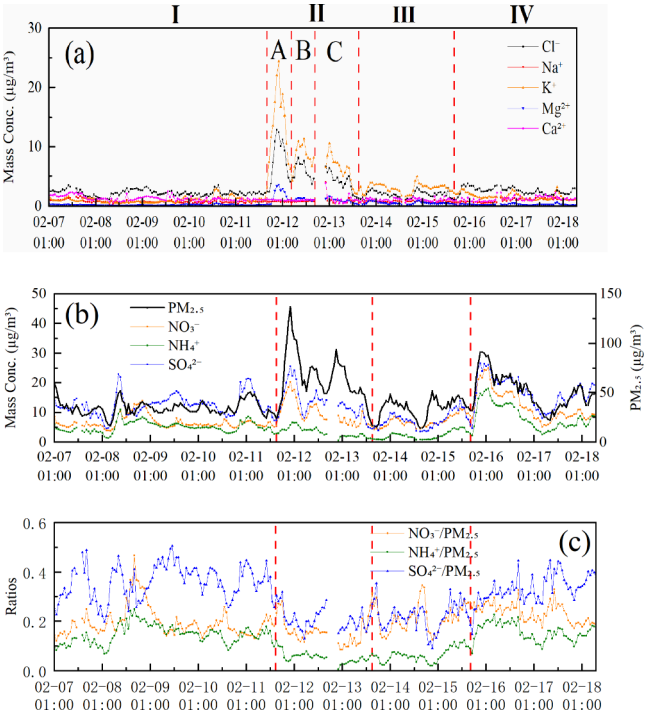

Figure 3. Hourly variations in the mass concentrations of particulate matter, concentrations of water-soluble inorganic ions in $PM_{2.5}$, and the ratio of water-soluble ions to $PM_{2.5}$ during the observation period. (a) and (b) show the time series of conventional pollutants and anion and cation concentrations, while (c) illustrates the variation in the ratios of the main components SO_4^{2-}, NO_3^-, and NH_4^+ in $PM_{2.5}$.

(1:00 on Feb 7th -16:00 on Feb 11th) and IV (17:00 on Feb 15th -8:00 on Feb 18th), the concentrated discharge period II (17:00 on Feb 11th -16:00 on Feb 13th), and discharge impact period III (17:00 on Feb 13th -17:00 on Feb 15th).

During the concentrated discharge period II, the mass concentrations of $PM_{2.5}$ and PM_{10} were 65.6 ± 25.0 $\mu g/m^3$ and

https://doi.org/10.1021/acsomega.4c03237
ACS Omega 2024, 9, 37754−37762

89.8 ± 37.0 $\mu g/m^3$, respectively, nonexceeding 75 $\mu g/m^3$ for $PM_{2.5}$ and 150 $\mu g/m^3$ for PM_{10} (24-h average) according to the National Ambient Air Quality Standards of China (NAAQS) released in 2012 by the Ministry of Environmental Protection (MEP) of the People's Republic of China. It is important to note that these levels are considered very high by most international standards. For instance, the United States Environmental Protection Agency (EPA) sets the 24-h average standards for $PM_{2.5}$ at 35 $\mu g/m^3$ and for PM_{10} at 150 $\mu g/m^3$. The European Union (EU) sets the 24-h limit for PM_{10} at 50 $\mu g/m^3$. Japan's 24-h standard for $PM_{2.5}$ is 35 $\mu g/m^3$, and the United Kingdom follows the EU's 24-h limit for PM_{10}. Comparing these standards to the observed levels of $PM_{2.5}$ and PM_{10} concentrations in our study region highlight the severe air quality issues caused by fireworks discharge.

The background concentrations of K^+ were determined based on nondischarge periods I (spanning approximately 5 days), with a measured background concentration of 1.04 ± 0.43 $\mu g/m^3$. Recent regulations have banned the use of wood and biomass fuels for heating within the area, thereby substantially reducing K^+ emissions from these sources. This policy has ensured that the relatively low background concentrations of K^+ are minimally influenced by local emissions during the winter season. Consequently, the observed elevated levels of K^+ during the study period can be attributed primarily to fireworks discharge. This attribution is supported by the consistent use of K^+ as an indicator ion to assess the intensity of fireworks discharge events, reinforcing its reliability as a marker in such environmental studies.[16,17]

Fireworks discharge events primarily occurred during the concentrated discharge period II (corresponding to periods A–C in Figure 3a). The most intense discharge occurred during the period of New Year's Eve and the early morning of the first day of the year, specifically during the A event (from 16:00 on Feb 11th to 6:00 on Feb 12th). During this period, the peak concentration of K^+ reached 21.5 $\mu g/m^3$, and the $PM_{2.5}$ concentration rapidly increased from 30.0 $\mu g/m^3$ to 136.8 $\mu g/m^3$, gradually decreasing to background levels as pollutants dispersed. The fireworks intensity of events B and C was relatively low compared to A, and the average concentrations of $PM_{2.5}$ and K^+ were much lower than event A with $PM_{2.5}$ concentrations of 63.6 $\mu g/m^3$ (B) and 54.6 $\mu g/m^3$ (C), and K^+ concentrations of 8.93 $\mu g/m^3$ (B) and 6.16 $\mu g/m^3$ (C), respectively.

The intensity of fireworks during the discharge impact period III was further decreased, resulting in a gradual decrease in the concentrations of K^+. During period III, the average $PM_{2.5}$ concentration was 35.0 ± 10.5 $\mu g/m^3$, and the PM_{10} concentration was 50.8 ± 17.5 $\mu g/m^3$. In comparison, during the nondischarge period I, the average $PM_{2.5}$ concentration was 34.5 ± 7.18 $\mu g/m^3$, and the average PM_{10} concentration was 49.0 ± 12.0 $\mu g/m^3$. These increases, although slight, were found to be statistically significant based on t tests ($PM_{2.5}$: $t = -3.687$, $p = 0.0003$; PM_{10}: $t = -3.957$, $p = 0.0001$), affirming that the observed higher concentrations are not only slightly but also significantly higher. In the nonfireworks combustion period IV, despite the elevated levels of $PM_{2.5}$ and PM_{10}, recorded at 52.1 ± 17.9 $\mu g/m^3$ and 84.1 ± 25.2 $\mu g/m^3$ respectively, the concentration of K^+ was notably low, at only 1.60 $\mu g/m^3$. This starkly contrasts with the concentrated discharge periods, where K^+ concentrations were exceptionally high, highlighting the distinct sources and dynamics of particulate matter across different periods."

3.3. Analysis of Water-Soluble Inorganic Ion Balance in $PM_{2.5}$.

Ion balance calculations are frequently used to investigate the acid–base balance of the ions in aerosol or other environmental samples. While ion balance calculations may not be directly applicable to emissions analysis, they nonetheless offer substantial insights. These calculations efficiently illustrate the charge distribution among anions and cations in aerosols, facilitating a straightforward inference of the aerosol's physicochemical properties and conditions. This capability to elucidate fundamental aerosol characteristics succinctly is a primary reason for the widespread adoption of ion balance calculations in atmospheric science research. Cation equivalent (CE) and anion equivalent (AE) are used here to calculate the charge balance:

$$\sum \mathrm{CE} = \frac{N_a^+}{23} + \frac{NH_4^+}{18} + \frac{K^+}{39} + \frac{M_g^{2+}}{12} + \frac{C_a^{2+}}{20} \quad (1)$$

$$\sum \mathrm{AE} = \frac{Cl^-}{35.5} + \frac{NO_3^-}{62} + \frac{SO_4^{2-}}{48} \quad (2)$$

The relationships between the anions and cations are shown graphically in Figure 4. The correlation coefficient for the cation vs anion concentration data was higher to 0.98, and the simple explanation for this is that the ions share a similar formation pathway. The slope(cation/anion) of the linear regression for $PM_{2.5}$ samples was 1.09. As most of the known major ions except carbonate and bicarbonate were measured, the anions deficits are best explained by the presence of those ions.[9] The result implies that the aerosol particles are slightly alkaline. Table 1 provides the concentrations of various water-soluble inorganic ions in $PM_{2.5}$, along with their proportions in total water-soluble inorganic ions. According to the table, the

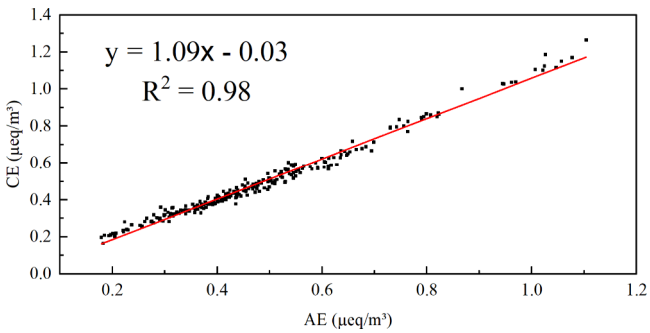

Figure 4. Ionic balance between cations (AE) and anions (CE) in $PM_{2.5}$.

Table 1. Concentrations and Percentages of Water-Soluble Inorganic Ions in $PM_{2.5}$

Ions	Mean, $\mu g/m^3$	Range, $\mu g/m^3$	Average proportion of total water-soluble inorganic ions, %	Average proportion of $PM_{2.5}$, %
Na^+	0.82	0.32–4.01	2.11 ± 1.4	2.01 ± 1.15
NH_4^+	5.11	0.61–18.1	14.7 ± 5.25	11.7 ± 5.49
K^+	2.73	0.47–21.5	7.70 ± 6.57	5.51 ± 4.10
Mg^{2+}	0.47	0.02–3.62	1.39 ± 1.12	1.02 ± 0.59
Ca^{2+}	1.24	0.02–3.91	3.32 ± 5.51	3.12 ± 1.63
Cl^-	2.83	1.01–12.9	8.07 ± 2.65	6.31 ± 1.89
SO_4^{2-}	12.2	3.63–26.7	35.2 ± 8.27	29.2 ± 10.0
NO_3^-	9.06	3.89–25.7	26.2 ± 5.02	20.7 ± 5.32

https://doi.org/10.1021/acsomega.4c03237
ACS Omega 2024, 9, 37754–37762

proportion of total water-soluble inorganic ions in $PM_{2.5}$ during the observation period averaged 79.6 ± 10.3%. Three dominant ions were identified during the observation period, including SO_4^{2-}, NO_3^-, and NH_4^+, and the sum concentration accounts for approximately 76.1 ± 13.5% of the total ions and 61.6 ± 11.2% of the $PM_{2.5}$. In addition, the concentrations of SO_4^{2-} and NO_3^- were observed significant increases in both particulate matter accumulation events and fireworks display events, respectively, and the characteristics will be discussed separately later.

The higher concentrations of NH_4^+ were observed in the particulate matter accumulation events during the nonconbustion period IV. Previous studies have shown that elevated NH_3 levels are typically found in summer, primarily due to the volatilization of fertilizers from surrounding farmlands and local sanitary wastes.[18] On the other hand, increased NH_4^+ levels in winter may result from the conversion of NH_3 at lower temperatures and higher concentrations of acid species like sulfate and nitrate.[19] This study also observed consistently high levels of NH_4^+, showing a significant 700% increase within a short period under relatively low temperatures (12.3 ± 2.51 °C) and high relative humidity (78.4 ± 18.8%). Correlation analysis revealed that NH_4^+ may share formation pathways with SO_4^{2-} and NO_3^-, exhibiting high correlation coefficients of 0.74 (NH_4^+ and SO_4^{2-}) and 0.64 (NH_4^+ and NO_3^-), respectively. In addition, the medium coefficient was observed between NH_3 and ambient temperature, indicating that the atmospheric concentration of NH_3 was significantly impacted by temperature variation. Notably, there seems to be no direct correlation between NH_4^+ and NH_3, suggesting that the complex results could potentially be attributed to the high chemical reactivity of NH_3.

Previous research has indicated that fireworks contain oxidants such as potassium perchlorate and potassium nitrate,[11,17] as well as coloring agents like Mg, Ba, and Cu.[20,21] The concentrations of K^+, Mg^{2+}, and Cl^- simultaneously arise very substantially during the concentrated discharge period II, and a strong relationship was obtained from K^+ vs Mg^{2+} and K^+ vs Cl^- (with R^2 values of 0.97 and 0.83, respectively), indicating a significant impact of fireworks discharge rather than biomass burning.[22] This finding is consistent with studies conducted in Beijing,[23] Shanghai,[24] and Xi'an.[12]

Three fireworks discharge events (A, B, and C) were observed in the concentrated discharge period II according to the peak concentrations of indicator K^+ with 21.5 $\mu g/m^3$, 11.4 $\mu g/m^3$, and 10.5 $\mu g/m^3$, respectively, which were 20.7, 10.9, and 10.1 times higher than the background concentrations. Additionally, the highest concentrations of Mg^{2+} and Cl^- reached 3.62 $\mu g/m^3$ and 12.9 $\mu g/m^3$ in the most intense discharge event A, respectively, which were 15.7 and 5.71 times higher than the background concentrations. And the SO_4^{2-} and NO_3^- showed the highest concentrations in this period, approximately accounting for 52.6% of the total ions and 35.2% of $PM_{2.5}$. Furthermore, a strong correlation was obtained from SO_4^{2-} and NO_3^-(R^2= 0.60), suggesting that they may share similar formation pathways.

The concentrations of SO_4^{2-} and NO_3^- were quite consistent with the $PM_{2.5}$ variations in different stages (II–IV), and correlations were calculated for each stage (Figure 5). The correlation coefficients (R^2) between NO_3^- and SO_4^{2-} for the four periods were 0.03, 0.60, 0.76, and 0.84, respectively. The increasing R^2 values indicate that the consistency of the

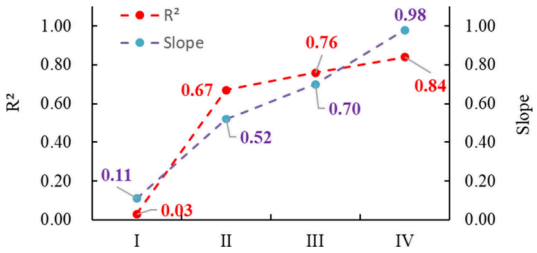

Figure 5. Coefficients (R^2) and slopes of linear regressions between SO_4^{2-} and NO_3^- in $PM_{2.5}$ during four firework burning phases (I Nondischarge period; II Concentrated discharge period; III Discharge impact period; IV Nondischarge period).

sources of SO_4^{2-} and NO_3^- rapidly increased from period I to IV, particularly during the particulate matter accumulation events. The nondischarge periods I and IV were characterized by higher SO_4^{2-} levels, reaching 12.4 ± 3.50 $\mu g/m^3$ and 17.3 ± 4.89 $\mu g/m^3$, respectively. The high coefficient (0.84) during the accumulation event suggests that SO_4^{2-} and NO_3^- in the nondischarge period IV primarily originated from precursor oxidation.[10] Conversely, the low coefficient (0.03) during the nondischarge period I may indicate unrelated conversion pathways and precursor sources. However, there was a significant increase in the intensity of NO_3^- accumulation during the particulate matter accumulation, with a higher slope (0.98). This finding is consistent with previous research conducted during pollution episodes in the Beijing area, indicating a shift from coal combustion pollution to mobile emission pollution, likely attributable to the cumulative emissions from vehicle exhaust.[25]

The concentrated discharge stage (II) yielded a moderate slope (0.52) and a high correlation coefficient (R^2 = 0.67) in the linear regression equation between SO_4^{2-} and NO_3^-. This stage, characterized by lower wind speeds (0.68 m/s), hindered the dispersion of pollutants and limited their transfer from surrounding areas to the monitoring site. The elevated coefficient suggests a potential shared origin for both SO_4^{2-} and NO_3^-. However, this high correlation could also be attributed to meteorological factors. For instance, a temperature inversion can create a stable layer that inhibits the vertical mixing of the air, leading to the accumulation of pollutants in the lower atmosphere. Under such meteorological conditions, although the formation processes of SO_4^{2-} and NO_3^- might be independent, their concentrations can increase simultaneously, resulting in a high correlation.

Previous studies have highlighted the significant role of transition metal ions (TMIs) in catalyzing the heterogeneous oxidation of SO_2, particularly under high relative humidity (RH), low pH, and low oxidant concentrations, conditions commonly found in industrial regions like the North China Plain.[26−28] Specifically, sulfate formation is enhanced in humid environments (RH > 40%) where water vapor accelerates SO_2 conversion, and low pH levels from acidic aerosols provide an optimal environment for TMI catalysis. Fireworks combustion releases various TMIs that can enhance sulfate formation.[27−29] However, our study's aerosol ion balance shows a slightly alkaline nature, suggesting TMI-catalyzed oxidation may not be dominant. Instead, the high sulfate levels are likely due to NO_2 and O_3 oxidation. During the concentrated discharge period (II), the average O_3 concentration was significantly lower (33.9 $\mu g/m^3$) compared to nondischarge periods I (42.1 $\mu g/m^3$) and IV (51.8 $\mu g/m^3$), and discharge impact period III

https://doi.org/10.1021/acsomega.4c03237
ACS Omega 2024, 9, 37754−37762

(50.0 $\mu g/m^3$), probably indicating O_3 consumption in sulfate formation.

Assuming that the increase in sulfate concentration is primarily caused by the oxidation reaction between precursor substances and O_3, ignoring the influences of environmental conditions such as relative humidity, temperature, and ionic strength, this study attempts to estimate the amount of O_3 involved in the oxidation reaction. Based on the chemical equation $SO_2 + O_3 + H_2O \rightarrow 2H^+ + SO_4^{2-}$, during the concentrated discharge period (II), the increase in sulfate concentration consumed approximately 0.35 $\mu g/m^3$ of O_3. Meanwhile, the concentration of O_3 during this period decreased by about 9.7 $\mu g/m^3$ compared to the nondischarge periods (I). Therefore, the O_3 used for the production of SO_4^{2-} accounts for only 3.61% of the total O_3 loss.

Although this estimation ignores several environmental factors,[30,31] the results suggest that the formation of SO_4^{2-} during the concentrated discharge period (II) is significantly influenced by O_3. However, the substantial decrease in O_3 is not primarily caused by the formation of SO_4^{2-} but is likely due to titration by NO_x or other chemical pathways. This analysis underscores the importance of understanding the reaction kinetics between O_3 and SO_4^{2-} for accurately assessing atmospheric pollution processes.

The gas-phase precursors of SO_2 and NO_2 originating from fireworks discharge significantly elevated the concentrations of SO_4^{2-} and NO_3^- within a few hours during the concentrated discharge stage of fireworks. These findings can be further elucidated by assessing the sulfur oxide conversion rate (SOR) and the conversion rate of nitrogen oxides (NOR). The SOR displayed an inverse pattern compared to the NOR, with a higher SOR (0.80) and lower NOR (0.28) observed during the concentrated discharge phase II. However, the NOR increased to 0.45 during the particulate accumulation event, indicating a distinct trend influenced by meteorological conditions.

Typically, higher relative humidity enhances the conversion of NO_2 to NO_3^-, leading to higher NOR values. During the concentrated discharge period (II), the relative humidity was 92.5%, which was significantly higher than the 78.3% observed during the nondischarge period IV. However, our findings show that despite the lower relative humidity in period IV, NOR still increased. This probably suggests that relative humidity might not be the primary factor controlling this conversion. Instead, the observed increase in NOR during period IV is likely attributed to the higher O_3 concentration (51.8 $\mu g/m^3$) compared to period II (33.9 $\mu g/m^3$). This probably indicates that the oxidation of NO_2 by O_3 had a more significant impact on NO_3^- formation than the meteorological conditions. Wind speeds during the concentrated fireworks discharge stage (II) and nondischarge period IV were measured at 0.68 ± 0.48 m/s and 1.03 ± 0.88 m/s, respectively. The relatively low wind speeds in both stages minimized the influence from the surrounding discharge area and accentuated the impact of local emissions. Consequently, both SO_4^{2-} and NO_3^- showed simultaneous increases alongside the rise in $PM_{2.5}$ concentrations.

$$\mathrm{SOR} = \frac{n - \mathrm{SO_4^{2-}}}{(n - \mathrm{SO_4^{2-}} + \mathrm{SO_2})} \quad (3)$$

$$\mathrm{NOR} = \frac{n - \mathrm{NO_3^-}}{(n - \mathrm{NO_3^-} + \mathrm{NO_2})} \quad (4)$$

3.4. Contribution of Fireworks to $PM_{2.5}$.

Significant variations in K^+ concentrations during the study underscore the severe air quality impacts of fireworks events. K^+ levels rose sharply alongside $PM_{2.5}$, SO_4^{2-} and NO_3^- concentrations during the concentrated discharge period II, peaking rapidly and subsequently returning to background levels. These observations indicate substantial fluctuations in $PM_{2.5}$ concentrations due to fireworks, with three distinct discharge events (Periods A to C) identified based on K^+ concentrations (Figure 6).

The contribution of total particle mass, SO_4^{2-} and NO_3^- emitted by fireworks to $PM_{2.5}$ can be calculated without the impact of postfireworks accumulations. The principles and assumptions for the estimation are as follows: (1) the K^+ concentration, after background subtraction, originates solely from the firework burning; (2) $PM_{2.5}$, SO_4^{2-} and NO_3^- after background subtraction, also originates solely from the firework burning and could be considered as the sum of two fractions—one from direct firework burning and the other from secondary formation; (3) the ratios of $PM_{2.5}/K^+$, SO_4^{2-}/K^+, and NO_3^-/K^+ from direct firework burning are constant, This implies that the changes in these components are linear with the changes in K^+ concentration.[23]

The total contribution of fireworks discharges to $PM_{2.5}$ was obtained using the regression equations between $PM_{2.5}$, SO_4^{2-}, NO_3^- and K^+(with background levels subtracted, calculated from the nondischarge period I) during fireworks discharge event A. The detailed regression equations are presented in Figure 7. Significant relationships (R^2) were observed between $PM_{2.5}$, SO_4^{2-}, NO_3^-, and K^+ during the increase and decrease process of event A, with R^2 values of 0.94 for $PM_{2.5}$ and K^+, 0.87 for SO_4^{2-} and K^+, 0.81 for NO_3^- and K^+, respectively. These strong correlations provide compelling evidence that $PM_{2.5}$, SO_4^{2-} and NO_3^- were significantly impacted by fireworks discharges.

The corresponding concentration of $\Delta[PM_{2.5}]$ was calculated to be 99.2 $\mu g/m^3$ based on the $\Delta[K^+]$, accounting for approximately 72.5 ± 25.6% of $PM_{2.5}$. This implies a significant contribution from the fireworks to $PM_{2.5}$. Similarly, the concentrations of $\Delta[SO_4^{2-}]$ and $\Delta[NO_3^-]$ were calculated to be 21.1 $\mu g/m^3$ and 14.8 $\mu g/m^3$ respectively, based on the $\Delta[K^+]$, accounting for approximately 15.4 ± 18.7% and 10.9 ± 12.3% of $PM_{2.5}$.

The analysis of fireworks discharge event A highlights the profound impact of fireworks on air quality, particularly the significant contributions to $PM_{2.5}$, sulfate, and nitrate levels. Figure 7 reveals that at the onset of the firework discharge, nitrate concentrations are significantly impacted by the fireworks. As the intensity of the discharge increases, sulfate concentrations surpass those of nitrate, gradually becoming the predominant pollutant. The steeper slope of sulfate in the regression analysis indicates a more substantial formation of sulfate compared to nitrate with increasing firework intensity.

These findings suggest different formation mechanisms and environmental behaviors for sulfate and nitrate. This underscores the necessity of implementing targeted emission control strategies during fireworks events to mitigate their adverse environmental and health effects. Future research should focus on detailed chemical pathways and the long-term impacts of these episodic emissions on urban air quality.

4. CONCLUSIONS

This study provides a comprehensive analysis of the impact of fireworks on air quality during the Spring Festival in Nanchang

https://doi.org/10.1021/acsomega.4c03237
ACS Omega 2024, 9, 37754−37762

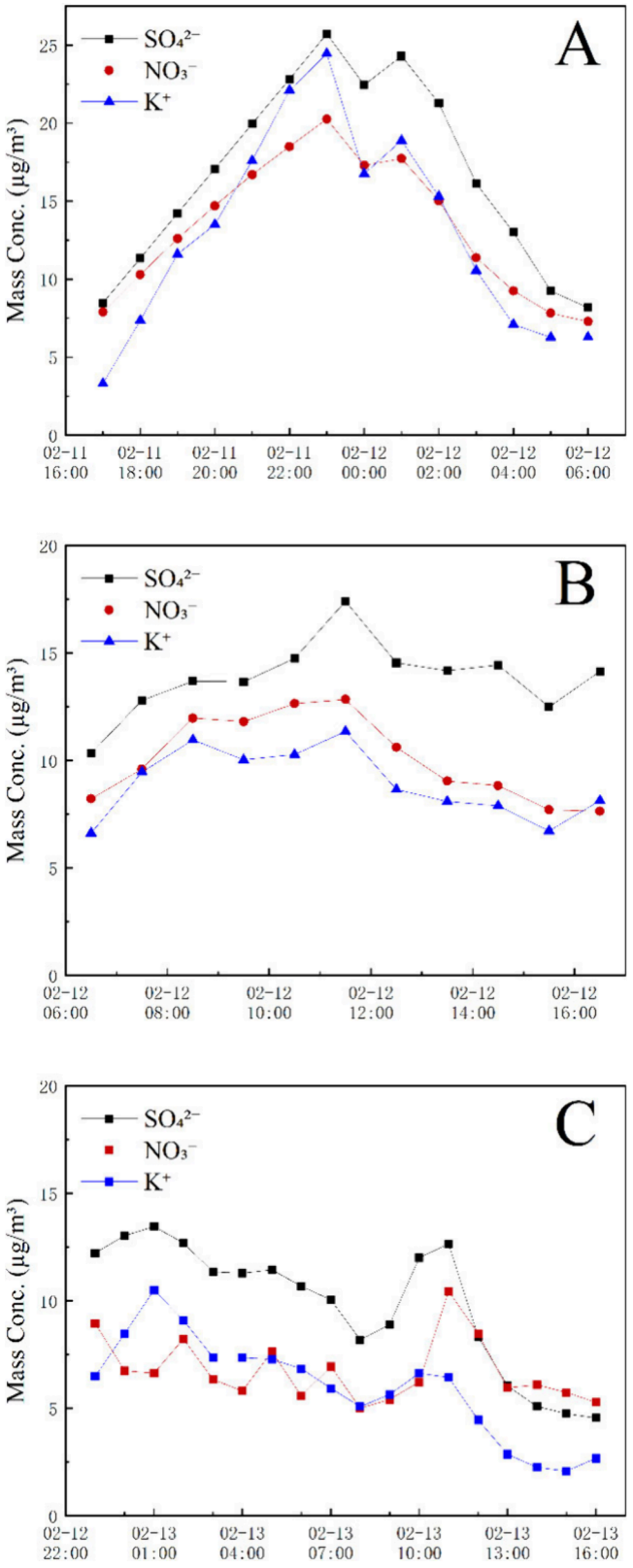

Figure 6. Hourly concentrations of K^+, SO_4^{2-}, and NO_3^- in $PM_{2.5}$ during three firework-burning periods: A, B, and C (fireworks discharge event).

City. The findings demonstrate a significant increase in $PM_{2.5}$, K^+, SO_4^{2-}, and NO_3^- concentrations due to fireworks emissions.

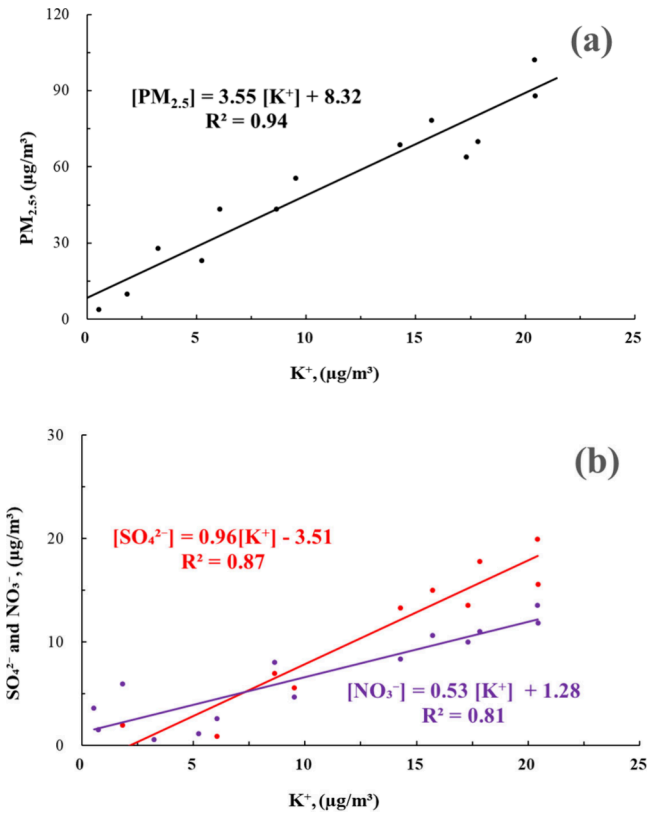

Figure 7. Regression equations of $PM_{2.5}$ with K^+, SO_4^{2-} with K^+, and NO_3^- with K^+ during the concentrated discharge period II of event A, after background subtraction (background values are the averages from the nonfirework discharge period I). (a) represents the regression equation of $PM_{2.5}$ with K^+, and (b) shows the regression equations of SO_4^{2-} and NO_3^- with K^+.

During the most intense discharge event, concentrations of K^+, $PM_{2.5}$, and PM_{10} were found to be 20.7, 3.63, and 3.32 times higher than background levels, respectively. The contribution of fireworks to $PM_{2.5}$ was significant, accounting for approximately 72.5 ± 25.6% of the total $PM_{2.5}$. This underscores the substantial role of fireworks in air pollution during festival periods.

Furthermore, the study revealed that the concentrations of $\Delta[SO_4^{2-}]$ and $\Delta[NO_3^-]$ were 21.1 $\mu g/m^3$ and 14.8 $\mu g/m^3$, respectively, contributing approximately 15.4 ± 18.7% and 10.9 ± 12.3% to $PM_{2.5}$. The sharper increase in SO_4^{2-} compared to NO_3^- indicates different formation mechanisms, with SO_4^{2-} the formation being more dominant during firework events.

These results highlight the urgent need for targeted emission control strategies during fireworks displays to mitigate their adverse environmental and health effects. Effective management and regulation of fireworks activities, along with real-time air quality monitoring, are crucial to protecting public health and improving urban air quality. Future research should focus on the detailed chemical pathways involved in secondary pollutant formation and assess the long-term impacts of such episodic emissions on urban environments.

AUTHOR INFORMATION

Corresponding Authors

Ruihe Lyu − *College of Marine Resources & Environment, Hebei Normal University of Science & Technology, Hebei Key*

https://doi.org/10.1021/acsomega.4c03237
ACS Omega 2024, 9, 37754−37762

Laboratory of Ocean Dynamics, Resources and Environments, Qinhuangdao Key Laboratory of Marine Habitat and Resources, Qinhuangdao 066004, China; orcid.org/0000-0003-2679-0250; Email: Lrh3954@hevttc.edu.cn

Mingbiao Luo − *State Key Laboratory of Nuclear Resources and Environment, East China University of Technology, Nanchang 330013, China*; Email: mbluo@ecut.edu.cn

Authors

Changan Kang − *State Key Laboratory of Nuclear Resources and Environment, East China University of Technology, Nanchang 330013, China; Jiangxi Provincial Center for Environment Monitoring, Nanchang 330029, China*

Juanjuan Jia − *Jiangxi Provincial Center for Environment Monitoring, Nanchang 330029, China*

Min Liu − *Jiangxi Provincial Center for Environment Monitoring, Nanchang 330029, China*

Chenghua Qin − *China National Environmental Monitoring Centre, Beijing 100012, China*

Yanzhi Peng − *Jiangxi Provincial Center for Environment Monitoring, Nanchang 330029, China*

Bingwei Cao − *Jiangxi Provincial Center for Environment Monitoring, Nanchang 330029, China*

Caiyu Zou − *Jiangxi Provincial Center for Environment Monitoring, Nanchang 330029, China*

Yao Ma − *College of Marine Resources & Environment, Hebei Normal University of Science & Technology, Hebei Key Laboratory of Ocean Dynamics, Resources and Environments, Qinhuangdao Key Laboratory of Marine Habitat and Resources, Qinhuangdao 066004, China*

Complete contact information is available at: https://pubs.acs.org/10.1021/acsomega.4c03237

Notes

The authors declare no competing financial interest.

■ ACKNOWLEDGMENTS

This work was supported by the Natural Science Foundation of Hebei Province (B2022407001 and D2021407001). The authors would also like to express their appreciation for the funding received from the Joint Innovation Funding Project of China Uranium Industry Co., Ltd., and the State Key Laboratory of Nuclear Resources and Environment at the East China University of Technology (No. NRE2021-16).

■ REFERENCES

(1) Shou, Y.; et al. A review of the possible associations between ambient exposures and the development of Alzheimer's disease. *Ecotoxicology and Environmental Safety* **2019**, *174*, 344−352.

(2) Seinfeld, J. H.; Pandis, S.N. *Atmospheric Chemistry and Physics: From Air Pollution to Climate Change*; 2016; John Wiley & Sons.

(3) Wang, H.; et al. Water-soluble ions in atmospheric aerosols measured in five sites in the Yangtze River Delta, China: Size-fractionated, seasonal variations and sources. *Atmospheric environment* **2015**, *123*, 370−379.

(4) Guo, Q.; Chen, K.; Xu, G. Characteristics and Sources of Water-Soluble Inorganic Ions in in Urban Nanjing, China. *Atmosphere* **2023**, *14* (1), 135.

(5) Lin, Y. C.; et al. Heterogeneous formation of particulate nitrate under ammonium-rich regimes during the high-PM2.5 events in Nanjing, China. *Atmospheric Chemistry and Physics* **2020**, *20* (6), 3999−4011.

(6) Zhang, J.; et al. An evaluation of the thermodynamic equilibrium assumption for fine particulate composition: Nitrate and ammonium during the 1999 Atlanta Supersite Experiment. *Journal of Geophysical Research: Atmospheres* **2002**, *107* (D7), SOS 2-1−SOS 2-11.

(7) Xin, K.; Chen, J.; Soyol-Erdene, T. Formation mechanism and source apportionment of nitrate in atmospheric aerosols. *APN Science Bulletin* **2023**, *13* (1), 102−111.

(8) Jin, X.; et al. Significant contribution of organics to aerosol liquid water content in winter in Beijing, China. *Atmospheric Chemistry and Physics* **2020**, *20* (2), 901−914.

(9) Zhang, L.; et al. Prominent role of organics in aerosol liquid water content over the south-eastern Atlantic during biomass burning season. *EGUsphere* **2023**, *2023*, 1−28.

(10) Cheng, Y.; et al. The characteristics of Beijing aerosol during two distinct episodes: Impacts of biomass burning and fireworks. *Environ. Pollut.* **2014**, *185*, 149−157.

(11) Ying, M.; Dui, W.; Jian, L. The characteristics of and its water soluble ions during Spring Festival in PRD in 2012. *China Environmental Science* **2016**, *36* (10), 2890−2895.

(12) Wu, C.; et al. Chemical characteristics of haze particles in Xi'an during Chinese Spring Festival: Impact of fireworks burning. *Journal of Environmental Sciences* **2018**, *71*, 179−187.

(13) Zhao, Y.; et al. The effect of recent controls on emissions and aerosol pollution at city scale: A case study for Nanjing, China. *Atmos. Environ.* **2021**, *246*, 118080.

(14) Wu, J.; et al. Insights into particulate matter pollution in the North China Plain during wintertime: local contribution or regional transport? *Atmospheric Chemistry and Physics* **2021**, *21* (3), 2229−2249.

(15) Cheng, Y.; et al. Humidity plays an important role in the pollution in Beijing. *Environmental pollution* **2015**, *197*, 68−75.

(16) Ma, Y.; Wu, D.; Liu, J. The characteristics of and its water soluble ions during Spring Festival in PRD in 2012. *China Environmental Science* **2016**, *36* (10), 2890−2895.

(17) Jiang, Q.; et al. Aerosol composition and sources during the Chinese Spring Festival: fireworks, secondary aerosol, and holiday effects. *Atmospheric Chemistry and Physics* **2015**, *15* (11), 6023−6034.

(18) Teng, X.; et al. Identification of major sources of atmospheric NH_3 in an urban environment in northern China during wintertime. *Environ. Sci. Technol.* **2017**, *51* (12), 6839−6848.

(19) Cao, J.-J.; et al. Characterization of atmospheric ammonia over Xi'an, China. *Aerosol and Air Quality Research* **2009**, *9* (2), 277−289.

(20) Godri, K. J.; et al. Particulate oxidative burden associated with firework activity. *Environ. Sci. Technol.* **2010**, *44* (21), 8295−8301.

(21) Kong, S.; et al. The impacts of firework burning at the Chinese Spring Festival on air quality: insights of tracers, source evolution and aging processes. *Atmospheric Chemistry and Physics* **2015**, *15* (4), 2167−2184.

(22) Heng, Z.; et al. Characteristics of inorganic ions and organic components in from biomass burning. *Acta Scientiae Circumstantiae* **2017**, *37* (12), 4483−4491.

(23) Wang, Y.; et al. The air pollution caused by the burning of fireworks during the lantern festival in Beijing. *Atmos. Environ.* **2007**, *41* (2), 417−431.

(24) Yao, L.; et al. The effects of firework regulation on air quality and public health during the Chinese Spring Festival from 2013 to 2017 in a Chinese megacity. *Environ. Int.* **2019**, *126*, 96−106.

(25) Xu, Q.; et al. Nitrate dominates the chemical composition of during haze event in Beijing, China. *Sci. Total Environ.* **2019**, *689*, 1293−1303.

(26) Harris, E.; et al. Enhanced Role of Transition Metal Ion Catalysis During In-Cloud Oxidation of SO_2. *Science* **2013**, *340* (6133), 727−730.

(27) Li, H.; et al. Case study of spring haze in Beijing: Characteristics, formation processes, secondary transition, and regional transportation. *Environ. Pollut.* **2018**, *242*, 544−554.

(28) Yang, Y.; et al. Characteristics and formation mechanism of continuous extreme hazes in China: a case study in autumn of 2014 in the North China Plain. *Atmospheric Chemistry & Physics Discussions*, **2015**, *15* (7), 8165

(29) Jing, H.; et al. Wide-range particle characterization and elemental concentration in Beijing aerosol during the 2013 Spring Festival. *Environmental pollution* **2014**, *192*, 204−211.
(30) Yu, C.; et al. Ionic strength enhances the multiphase oxidation rate of sulfur dioxide by ozone in aqueous aerosols: Implications for sulfate production in the marine atmosphere. *Environ. Sci. Technol.* **2023**, *57* (16), 6609−6615.
(31) Guo, Z.; et al. Quantifying SO_2 oxidation pathways to atmospheric sulfate using stable sulfur and oxygen isotopes: laboratory simulation and field observation. *Atmospheric Chemistry and Physics* **2024**, *24* (4), 2195−2205.

https://doi.org/10.1021/acsomega.4c03237
ACS Omega 2024, 9, 37754−37762